Journal of Volcanology and Geothermal Research 402 (2020) 106991

Contents lists available at ScienceDirect

Journal of Volcanology and Geothermal Research

journal homepage: www.elsevier.com/locate/jvolgeores

Dating silica sinter (geyserite): A cautionary tale

Dakota M. Churchill [a,b,*], Michael Manga [a], Shaul Hurwitz [b], Sara Peek [c], Joseph M. Licciardi [d], James B. Paces [e]

[a] Department of Earth and Planetary Science, University of California, Berkeley, CA, USA
[b] U.S. Geological Survey, Moffett Field, CA, USA
[c] U.S. Geological Survey, Menlo Park, CA, USA
[d] Department of Earth Sciences, University of New Hampshire, Durham, NH, USA
[e] U.S. Geological Survey, Denver, CO, USA

ARTICLE INFO

Article history:
Received 22 May 2020
Received in revised form 25 June 2020
Accepted 30 June 2020
Available online 06 July 2020

Keywords:
Yellowstone
Hydrothermal
Sinter
Radiocarbon dating
Beryllium-10 dating
Uranium-series dating

ABSTRACT

We describe a new effort to date hydrothermal silica sinter deposits (geyserite) from the Upper Geyser Basin of Yellowstone National Park using ^{14}C of co-deposited organic matter, U-series and cosmogenic ^{10}Be methods. A majority of the samples were collected from stratigraphic sections, mainly at Riverside, Giant, and Castle Geysers. Ages obtained from 41 ^{14}C analyses range from modern to 12.1 cal ka BP. Nearly all the ^{14}C ages show inconsistencies with their stratigraphic positions, and several replicate ^{14}C analyses from the same sample result in significantly different ages. The $\delta^{13}C$ values of the organic material in the sinter range from −26.6‰ to −12.7‰. The more enriched values are attributed to microbial fixation of dissolved inorganic carbon (DIC), which has heavier $\delta^{13}C$ values and is ^{14}C-depleted relative to atmospheric CO_2, leading to an apparent older age. U-series analyses on 4 samples yielded ages between 2.2 and 7.4 ka. Large $^{230}Th/U$ age uncertainties in the sinter, due to low uranium concentrations along with elevated ^{232}Th and associated initial ^{230}Th, make these ages imprecise for use on Holocene deposits. A single cosmogenic ^{10}Be exposure age of 596 ± 18 ka is considerably older than the age of underlying rhyolite and is thus unreliable. This apparent old age results from contamination by meteoric ^{10}Be trapped in the opal that overprints the very small amount of cosmogenic ^{10}Be. By presenting the problems we encountered and discussing their probable cause, this paper highlights the difficulty in obtaining reliable, high-precision geochronological data necessary to use sinter deposits as paleoenvironmental and paleo-hydrothermal archives.

Published by Elsevier B.V.

1. Introduction

The hydrothermal system in Yellowstone National Park (YNP) consists of more than 10,000 diverse thermal features, including geysers and non-erupting springs and pools (Hurwitz and Lowenstern, 2014). A significant proportion of Yellowstone's iconic geysers are in the Upper Geyser Basin (UGB; Fig. 1). Thermal waters currently discharging in the UGB have elevated concentrations of chloride, sodium, and silica (Hurwitz et al., 2012). As thermal waters cool following discharge, the solubility of silica (SiO_2) decreases (Fournier, 1985), leading to precipitation of opal-A and deposition of siliceous sinter that forms geyser cones, domal mounds, and terraces (e.g., Jones and Renaut, 2003; Lynne, 2012; Campbell et al., 2015a), collectively termed geyserite. Repeated wetting and evaporation of surfaces and capillary effects are the main controls on the deposition, morphology, and microstructure within sinter deposits. As the sinter deposits evolve, particles of rock, plant matter, charcoal, pollen, and microbial filaments can be trapped (Lowe and Braunstein, 2003; Guidry and Chafetz, 2003; Lynne et al., 2017).

Most geysers worldwide formed following the last glaciation, as inferred by stratigraphy and the few radiometric ages of sinter deposits (Hurwitz and Manga, 2017). In Yellowstone, it is assumed that all geyser deposits post-date the Pinedale deglaciation of the Yellowstone Plateau (ca. 15 ka; Licciardi and Pierce, 2018), as older deposits are expected to have been removed by glacial erosion beneath the >1 km thick ice cap. Therefore, the organic material trapped in the sinter deposited by these geysers can provide abundant information on post-glacial environmental changes, if deposits can be successfully dated. The original goal of this study was to establish temporal correlations between hydrothermal activity in the UGB and post-glacial regional climate. We also wanted to address questions such as: How long does it take for a large geyser cone to form; how old are some of the largest geysers in the UGB; do any of the sinter deposits in the UGB pre-date the Pinedale deglaciation? To establish age correlations and address these questions, we applied radiocarbon (^{14}C) dating methods on a large number of silica sinter samples. We also applied U-series and cosmogenic ^{10}Be dating methods to a small subset of those samples. We have focused our

* Corresponding author at: University of California, Berkeley, CA, USA.
E-mail address: dchurchill@berkeley.edu (D.M. Churchill).

https://doi.org/10.1016/j.jvolgeores.2020.106991
0377-0273/Published by Elsevier B.V.

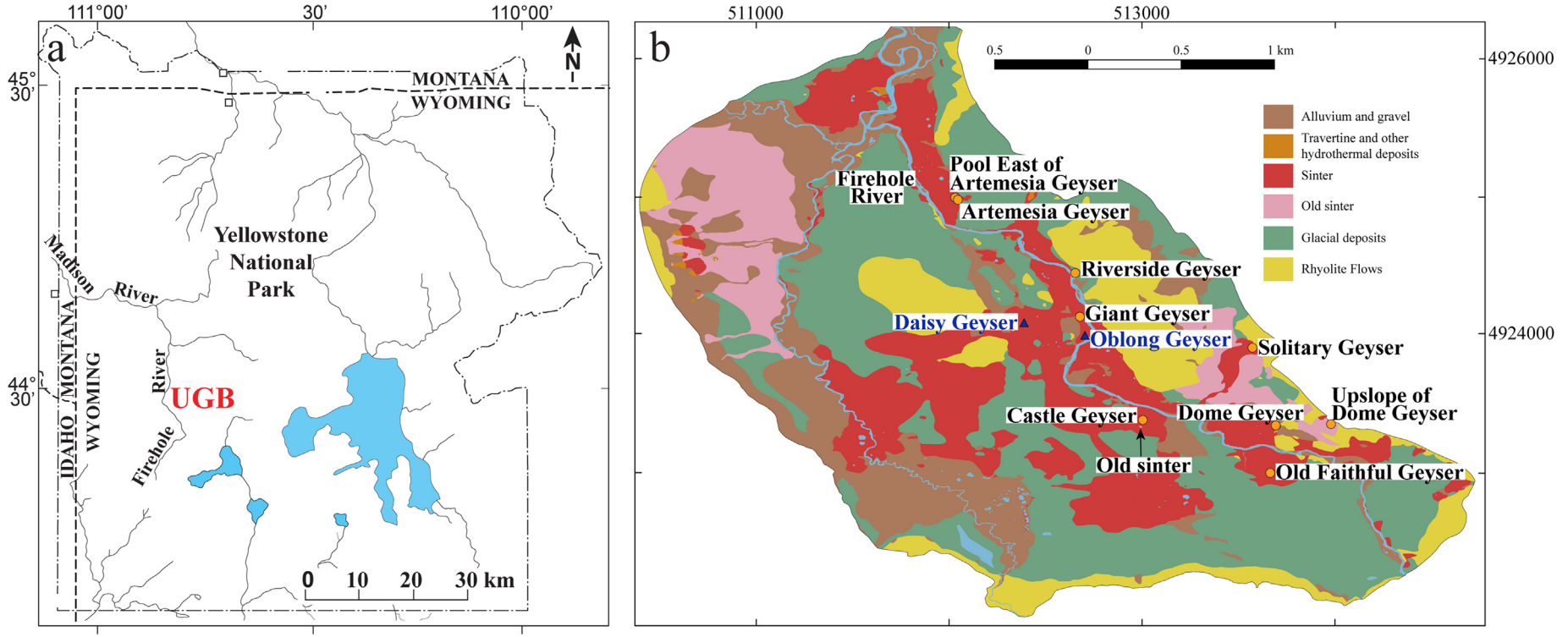

Fig. 1. a) Map of Yellowstone National Park (YNP) showing the location of the Upper Geyser Basin (UGB). b) Geologic map of the Upper Geyser Basin modified from Muffler et al. (1982) and digitized by Abedini et al. (2015). Coordinates are in Universal Transverse Mercator (UTM) Zone 12. The orange circles represent sample locations (Table 1). The blue triangles represent geysers from which uranium isotope data were used for comparison with uranium isotopes in sinter from Castle and Giant Geysers. Units are condensed from the original map; the separation between old sinter and sinter units is based on stratigraphy and sample and outcrop morphology, not on radiometric dating. Mapped "old sinter" below Castle Geyser (osi, Muffler et al., 1982) is indicated with an arrow. (For interpretation of the references to colour in this figure legend, the reader is referred to the web version of this article.)

Table 1
Radiometric ages for sinter samples from Upper Geyser Basin.

Sample ID	Location	Material dated	Carbon[a] (mg)	$\delta^{13}C$[b] (‰)	^{14}C Age[c,d] (cal ka BP)	U-Th Age (ka)	±2σ (ka)	^{10}Be Age (ka)	±2σ (ka)
UGB-TD-01	Old Faithful Geyser	Bulk[e]	0.4	–	7.6	–	–	–	–
UGB-TD-03B	Dome Geyser	Bulk	0.1	–	MODERN	–	–	–	–
UGB-TD-12[f]	Artemisia Geyser Outflow	Bulk	0.8	−23.4	4.1	–	–	–	–
UGB-TD-14	Artemisia Geyser Outflow	Bulk	0.1	–	9.6	–	–	–	–
UGB-TD-15	Pool East of Artemisia Geyser	Bulk	3.9	−24.1	4.6	–	–	–	–
UGB-TD-16	Pool East of Artemisia Geyser	Bulk	3.5	−12.7	9.8	–	–	–	–
UGB-TD-17	Pool East of Artemisia Geyser	Bulk	2.1	−23.6	1.3	–	–	–	–
UGB-TD-18	Pool East of Artemisia Geyser	Bulk	2.2	−22.2	0.5	–	–	–	–
UGB-TD-19	Riverside Geyser	Bulk	0.1	–	3.1	–	–	–	–
UGB-TD-20	Riverside Geyser	Bulk	3.2	−23.1	12.0	–	–	–	–
UGB-TD-21	Riverside Geyser	Bulk	0.3	−26.6	5.0	–	–	–	–
UGB-TD-23	Riverside Geyser	Bulk	1.8	−18.6	7.9	–	–	–	–
UGB-TD-24	Giant Geyser	Bulk	0.6	−17.0	3.8	–	–	–	–
UGB-TD-25	Giant Geyser	Bulk	0.1	–	5.1	–	–	–	–
UGB-TD-25A[g]	Giant Geyser	<20 μm[h]	2.2	−23.8	3.7	–	–	–	–
UGB-TD-25B	Giant Geyser	20–180 μm	0.2	–	6.6	–	–	–	–
UGB-TD-25C	Giant Geyser	>180 μm	<0.1	–	4.1	–	–	–	–
UGB-TD-26	Giant Geyser	Bulk	0.1	–	2.6	–	–	–	–
UGB-TD-27	Giant Geyser	Bulk	0.1	–	4.2	–	–	–	–
UGB-TD-27A	Giant Geyser	Bulk	–	–	–	7.4	6.3	–	–
UGB-TD-28	Giant Geyser	Bulk	3.3	−20.8	7.0	–	–	–	–
UGB-TD-29	Giant Geyser	Bulk	1.4	−14.7	9.4	–	–	–	–
UGB-TD-29A	Giant Geyser	Bulk	–	–	–	6.8	5.0	–	–
YGT18-27[i]	Castle Geyser	Bulk	–	–	–	–	–	596.0	18.0
UGB-TD-30B	Castle Geyser	Bulk	<0.1	–	8.0	–	–	–	–
UGB-TD-30C	Castle Geyser	<20 μm	2.2	−21.5	3.7	–	–	–	–
UGB-TD-30D	Castle Geyser	>180 μm	0.1	–	9.0	–	–	–	–
UGB-TD-31	Castle Geyser	Bulk	0.2	–	1.5	–	–	–	–
UGB-TD-31A	Castle Geyser	Bulk	<0.1	–	1.9	–	–	–	–
UGB-TD-31B	Castle Geyser	Needle	0.1	–	3.3	–	–	–	–
UGB-TD-32	Castle Geyser	Bulk	0.5	−23.6	2.9	–	–	–	–
UGB-TD-32A	Castle Geyser	Bulk	0.1	–	7.6	–	–	–	–
UGB-TD-33	Castle Geyser	Bulk	4.1	−20.5	10.0	–	–	–	–
UGB-TD-35	Castle Geyser	Bulk	2.8	−23.5	4.1	–	–	–	–
UGB-TD-35A	Castle Geyser	Bulk	1.6	−21.1	2.8	–	–	–	–
UGB-TD-35B	Castle Geyser	Charcoal	0.1	–	1.1	–	–	–	–
UGB-TD-37	Castle Geyser	Bulk	0.8	−18.0	4.2	–	–	–	–
UGB-TD-37A	Castle Geyser	Bulk	–	–	–	6.4	26.0	–	–
UGB-TD-37B	Castle Geyser	Charcoal	<0.1	–	2.0	–	–	–	–
UGB-TD-39	Castle Geyser	Bulk	1.1	−17.4	10.2	–	–	–	–
UGB-TD-39A	Castle Geyser	Bulk	–	–	–	2.2	7.9	–	–
UGB-TD-39B	Castle Geyser	Bulk	1.1	−19.4	12.1	–	–	–	–
UGB-TD-40	Solitary Geyser	Bulk	2.1	−18.1	2.6	–	–	–	–
UGB-TD-40A	Solitary Geyser	Bulk	1.4	−15.5	11.3	–	–	–	–
UGB-TD-43	Upslope of Dome Geyser	Bulk	3.1	−24.3	5.8	–	–	–	–
UGB-TD-43A	Upslope of Dome Geyser	Bulk	<0.1	–	7.3	–	–	–	–

[a] Calculated from the weight of combusted material and the measured percent carbon (Churchill et al., 2020).
[b] 2σ analytical uncertainty is ±0.2‰.
[c] Ages are calibrated using the CALIB 7.1 code (Stuiver and Reimer, 1993) and the UCIAMS atmospheric IntCal13 dataset (Reimer et al., 2013); uncalibrated ages can be found at Churchill et al. (2020).
[d] 2σ analytical uncertainty for all samples is ≤120 years, except for UGB-TD-30B and -43A which have uncertainties of 260 and 160 years, respectively.
[e] All organic material extracted from sample combined.
[f] Sample numbers collected at the same feature increase with increasing stratigraphic positions (from old to young).
[g] Letters (i.e. A, B, C, D) following the sample ID indicate replicates.
[h] Organic material sieved to <20 μm, 20–180 μm, and >180 μm.
[i] Sample collected adjacent to sample UGB-TD-30.

sampling on three of the largest geysers in the UGB: Riverside, Giant and Castle Geysers (Fig. 1b).

We were motivated by prior studies that applied Accelerator Mass Spectrometry (AMS) ^{14}C measurements to date organic material trapped in silica sinter samples from thermal areas worldwide (Lutz et al., 2002; Campbell et al., 2004; Lynne et al., 2005, 2008; Lynne, 2012; Campbell and Lynne, 2006; Foley, 2006; Howald et al., 2014; Lowenstern et al., 2016; Slagter et al., 2019; Muñoz-Saez et al., 2020). Uranium-thorium (Sharp et al., 2003; Paces et al., 2004, 2010; Maher et al., 2007), and uranium-lead (Neymark et al., 2002; Amelin and Back, 2006; Nemchin et al., 2006; Neymark and Paces, 2013) methods have been used to successfully date non-hydrothermal opal and chalcedony deposits associated with pedogenic or deeper vadose-zone environments, and electron spin resonance (ESR) methods have been used to date siliceous sinter (Chen et al., 1993). To the best of our knowledge, no previous attempts have been made to date sinter deposits using cosmogenic ^{10}Be exposure dating methods.

Despite the large number of samples that we dated and the multiple dating methods used, resulting ages scatter widely and are unreliable given their stated uncertainties and stratigraphic positions, or, in the case of U-series, have precisions too poor to allow detailed paleoenvironmental reconstruction. The goals of this paper are to present the data that we consider unreliable and communicate the complicating issues we faced in dating sinter using these geochronologic

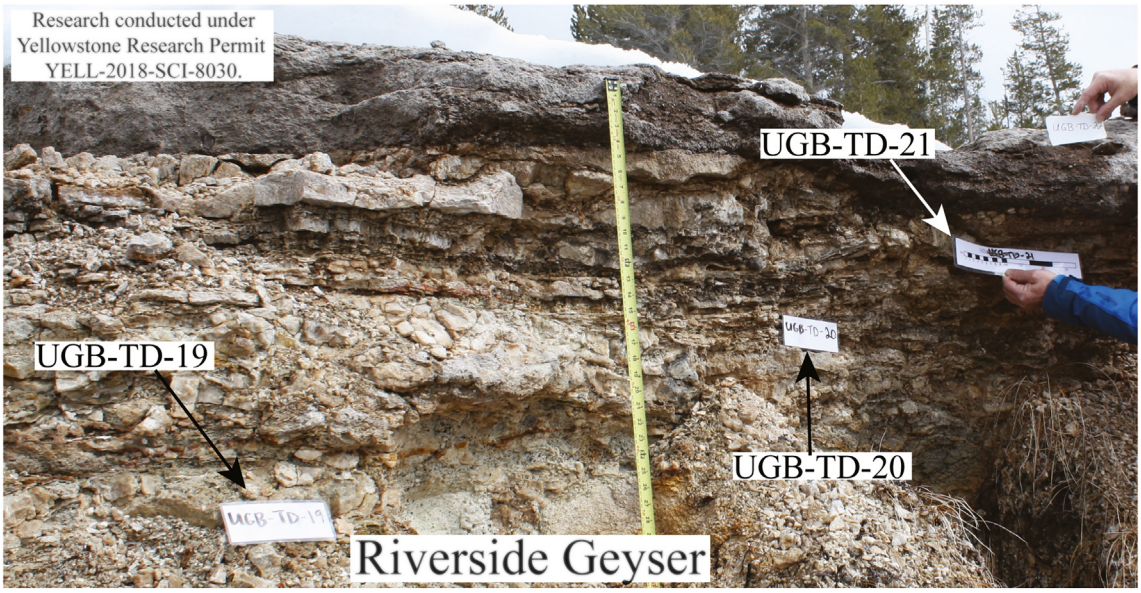

Fig. 2. Photos of Riverside Geyser looking to the east with labels indicating sample locations. UGB-TD-23 is not in view. Samples were collected under Research Permit YELL-2018-SCI-8030.

methods. All of the data collected during this study are summarized in condensed form here (Table 1) and are documented in more detail along with descriptions of the methods used for collecting, processing, and analyzing the sinter samples in a U.S. Geological Survey (USGS) data release (Churchill et al., 2020). It is our hope that highlighting the issues we encountered, and their probable causes, will provide a cautionary tale that helps inform and guide future studies that intend to use sinter deposits as paleoenvironmental and paleo-hydrothermal archives.

2. Methods

Forty-seven approximately fist-sized (400–800 g) sinter samples were collected from UGB geysers in April 2018, November 2018, and April 2019 at 9 separate locations (Fig. 1b). At Riverside (Fig. 2), Giant (Fig. 3), and Castle (Fig. 4) Geysers, samples were collected at approximately even spacings following the stratigraphy from the shield (old sinter) to the cone (young sinter). At Castle Geyser, the oldest exposed stratigraphic levels were mapped as "old sinter" (Fig. 1b; Muffler et al., 1982). Samples UGB-TD-30, -31, and -32 (Table 1) were collected from that old sinter unit (Fig. 4b); the stratigraphic relationship between these samples could not be determined. Sample UGB-TD-30 was collected directly adjacent to a sample dated previously by radiocarbon to 10.5 ka BP (Foley, 2006), which is calibrated to 12.4 ka BP.

Three samples from Castle Geyser (YGT18-27, -28, and -29—all adjacent to sample UGB-TD-30; Fig. 4b) and one sample from Solitary Geyser (Fig. 1b) were collected for ^{10}Be analysis. For these samples, additional information including horizon angle measurements and

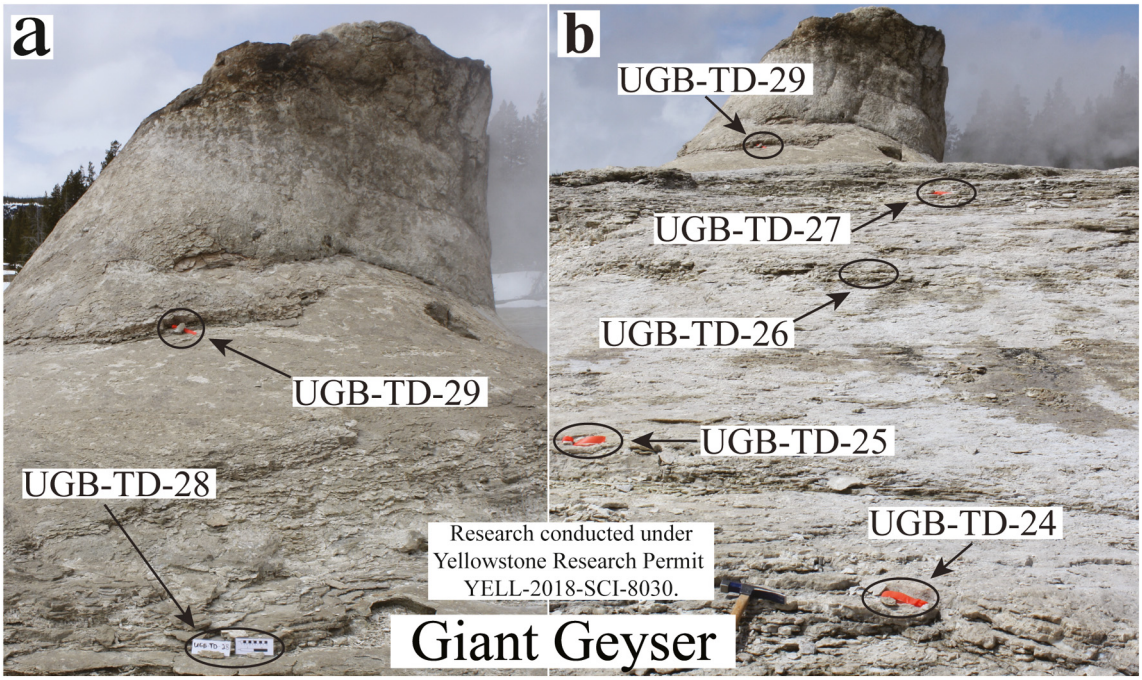

Fig. 3. a) and b) Photos of Giant Geyser looking to the west with labels indicating sample locations. Samples were collected under Research Permit YELL-2018-SCI-8030.

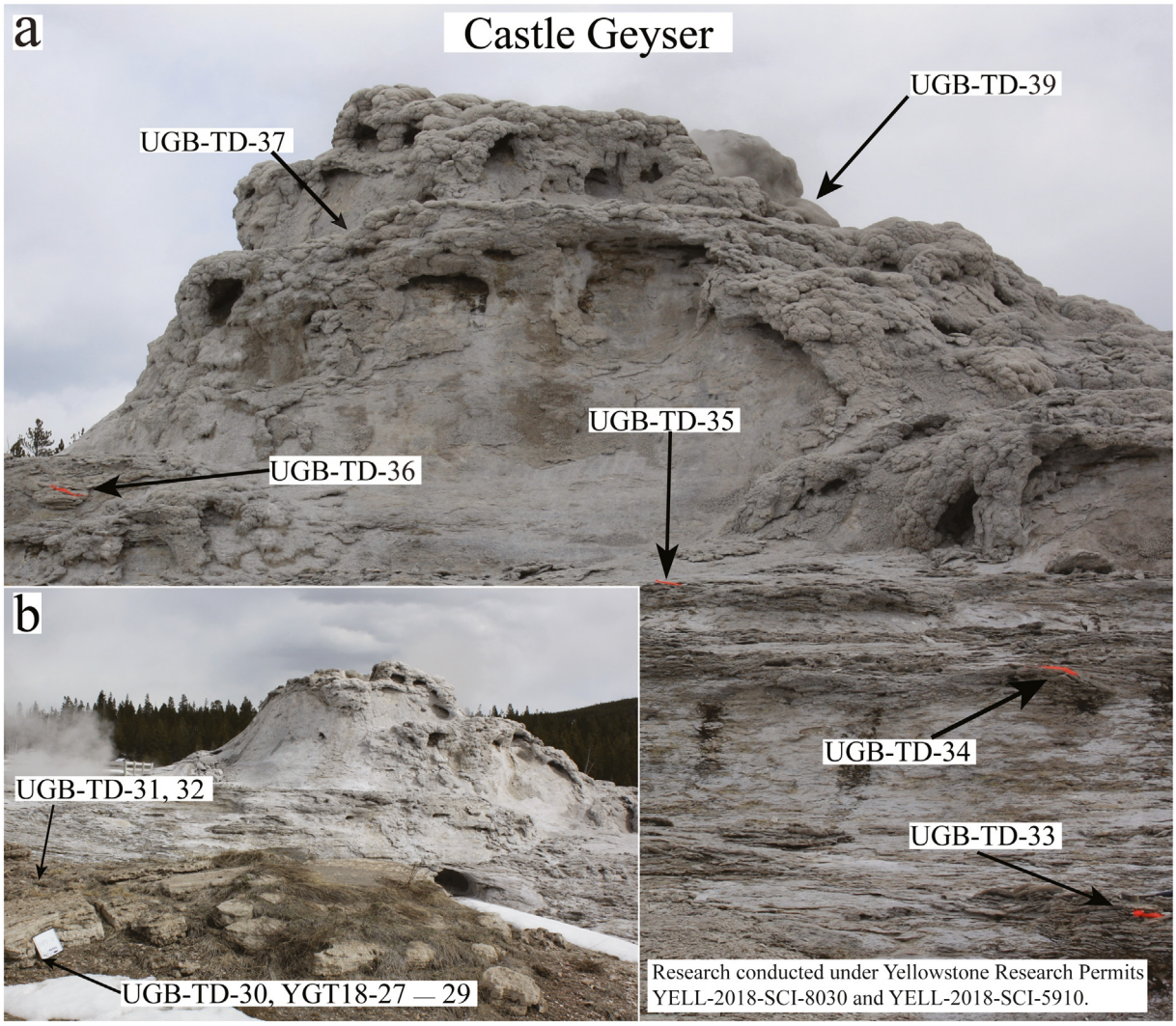

Fig. 4. Photos of Castle Geyser with labels indicating sample locations. a) looking to the southeast and b) looking to the northeast within an area mapped as "old sinter" (Muffler et al., 1982). Samples were collected under Research Permit YELL-2018-SCI-8030 and YELL-2018-SCI-5910.

strike and dip of rock surfaces were recorded to derive topographic shielding corrections for each sample site. Two sub-samples from Castle Geyser (UGB-TD-37A and -39A) and two sub-samples from Giant Geyser (UGB-TD-27A and -29A) were used for U-Th isotope analysis.

Organic material was separated from sinter samples for radiocarbon dating following established methods (Howald et al., 2014; Lowenstern et al., 2016; Slagter et al., 2019). Samples were processed until all inorganic carbonate, modern algae, and silicate material was removed. Of the 80 to 700 g of sinter collected per sample (most being 200–300 g), 100 to 300 g were processed in hydrofluoric acid (HF) to isolate organic carbon. The organic material was analyzed for ^{14}C and $\delta^{13}C$ at the Keck-Carbon Cycle Accelerator Mass Spectrometry Laboratory (Keck-CCAMS) at the University of California, Irvine. Radiocarbon ages were calibrated using the CALIB 7.1 code (Stuiver and Reimer, 1993) and the UCIAMS atmospheric IntCal13 dataset (Reimer et al., 2013). All radiocarbon ages given hereafter in this study have been calibrated to calendar years.

Samples were analyzed for U-Th isotopes at USGS laboratories in Denver, CO. Small fragments were cut and polished to enable microsampling. Sub-samples were obtained by drilling small pits or trenches that cut across microfabric elements, integrating material weighing 0.08–0.13 g. Resulting powders were digested using concentrated HF along with known amounts of a mixed ^{229}Th-^{233}U-^{236}U tracer solution. After evaporation, residues were re-dissolved with nitric acid (HNO_3) and centrifuged to ensure that all material went into solution in order to avoid laboratory U/Th fractionation. Purified salts of U and Th were obtained by ion chromatography using AG1 × 8 resin (Paces et al., 2020, supplement). All U—Th isotope measurements were made on a Thermo Finnigan™ Triton thermal-ionization mass spectrometer by dynamic peak-hopping different masses into a single discrete dynode secondary electron multiplier.

Beryllium was extracted from milled rock to produce BeO target material for AMS analysis following established geochemical procedures (Licciardi, 2000; Corbett et al., 2016). All chemical work was conducted in clean laboratory facilities at the University of New Hampshire. Opal was isolated from bulk sinter material by progressive etchings in a dilute solution of 2% HF/1% HNO_3; sample amounts were reduced considerably during these progressive etchings. Opal purity was assessed by measuring major cation concentrations via inductively coupled plasma-optical emission spectrometry (ICP-OES) at the Analytical and Technical Services lab at SUNY College of Environmental Science and Forestry in Syracuse, New York. ^{9}Be carrier (~0.2 mg) was added to the purified opal before digestion in concentrated HF. Beryllium was extracted from samples using ion-exchange chromatography, selective precipitation, and oxidation to BeO. The $^{10}Be/^{9}Be$ analyses were

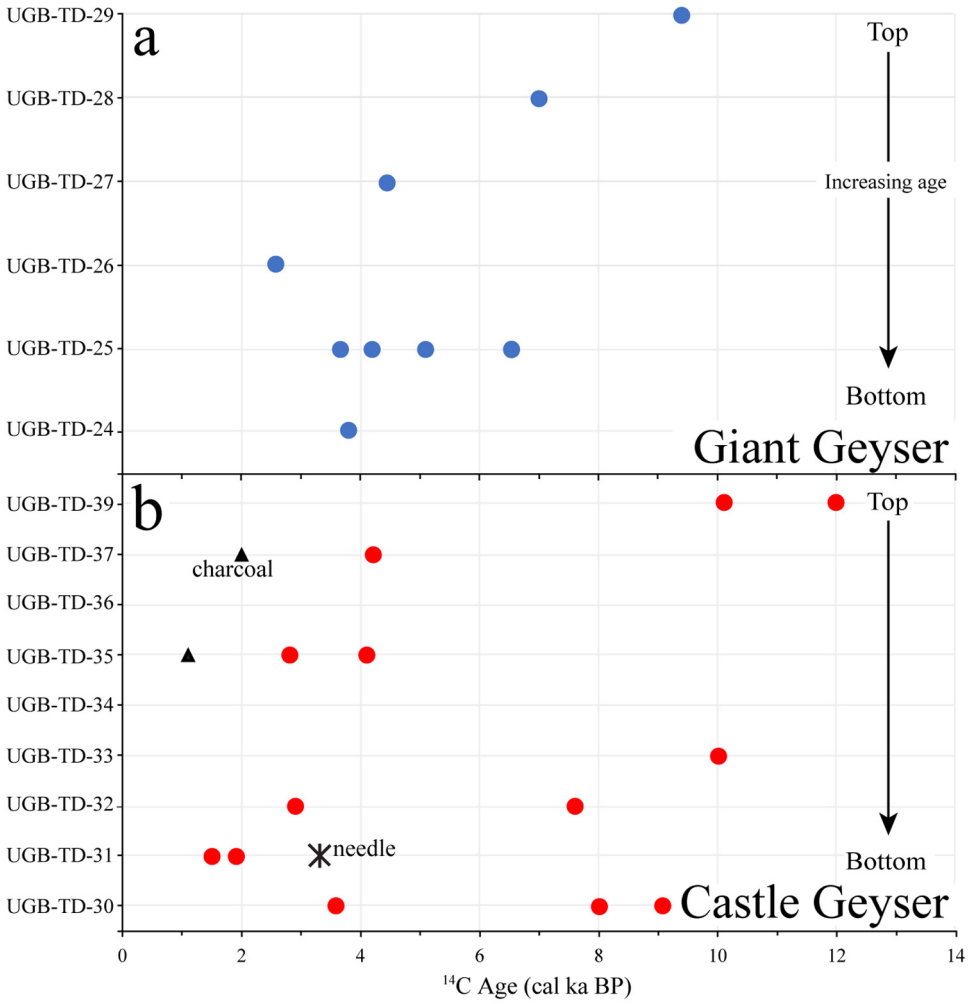

Fig. 5. Calibrated ^{14}C ages for a) samples from Giant Geyser and b) samples from Castle Geyser. Sample numbers for each feature increase with increasing stratigraphic positions (from old to young). The analytical uncertainty for the ^{14}C ages reported in Table 1 are smaller than the size of the symbols. All data are compiled in a USGS data release (Churchill et al., 2020).

performed at the Lawrence Livermore National Laboratory Center for Accelerator Mass Spectrometry (LLNL-CAMS).

3. Results

Complete datasets used to derive age estimates are available in a USGS data release (Churchill et al., 2020) with the resulting age estimates summarized in Table 1. Including sample replicates, where we dated different size fractions of the same sample, we report forty-one radiocarbon ages, four $^{230}Th/U$ ages, and one ^{10}Be age (Table 1). Age estimates are all reported in thousands of years (ka) with analytical uncertainties reported at the 95% confidence level ($\pm 2\sigma$). The radiocarbon data are presented as calibrated ages (cal ka before present - BP; 0 years BP = 1950 CE).

3.1. Carbon isotopes

The mass of carbon extracted and analyzed per sample ranged from 0.019 to 4.104 mg. Several samples had carbon yields that were insufficient for analysis. Only 23 of the 41 samples analyzed for radiocarbon also had enough carbon (>0.19 mg) for $\delta^{13}C$ analysis (Table 1). Radiocarbon ages of the 41 analyzed samples range from modern (zero-aged) to 12.1 cal ka BP with analytical uncertainties ranging from ± 15 to 260 years (median of ± 20 years). Higher uncertainties are associated with smaller carbon abundance in the sample. The range of $\delta^{13}C$ values for the 23 samples is from −26.6‰ to −12.7‰ (Table 1).

The ^{14}C ages from Riverside, Giant (Fig. 5a), and Castle (Fig. 5b) Geysers (Table 1) do not reflect their overall stratigraphic order. Furthermore, sample replicates from Giant and Castle Geysers vary by as much as ~5 cal ka (Table 1). Bulk organic material from sample UGB-TD-25 was sieved into 3 splits of <20 μm (UGB-TD-25A), 20–180 μm (UGB-TD-25B), and >180 μm (UGB-TD-25C). Ages for the bulk organic material and the three size fractions range from 3.7 to 6.6 cal ka BP, with no obvious correlation with size. Organic material from UGB-TD-30 was split into 4 sub-samples. Sample UGB-TD-30A had insufficient carbon for ^{14}C analysis; sample UGB-TD-30B was analyzed in bulk and yielded an age of 8.0 cal ka BP, whereas sieved samples UGB-TD-30C (<20 μm) and UGB-TD-30D (>180 μm) yielded ages of 3.7 and 9.0 cal ka BP, respectively. Replicates of sample UGB-TD-40 from Solitary Geyser differ by almost 9 cal ka. In all, ^{14}C ages of dispersed organic matter from Giant Geyser range from 2.6 to 9.4 cal ka BP and those from Castle Geyser range from 1.5 to 12.1 cal ka BP (Table 1). In two Castle Geyser samples, where charcoal pieces were separated and provided enough material for dating (UGB-TD-35 and -37), the ages of the charcoal are younger than the ages obtained from the respective bulk samples. However, the charcoal from UGB-TD-35 yielded an age (1.1 cal ka BP) that is younger than the age of the charcoal from UGB-TD-37 (2.0 cal ka BP), although UGB-TD-35 is stratigraphically lower than UGB-TD-37. In

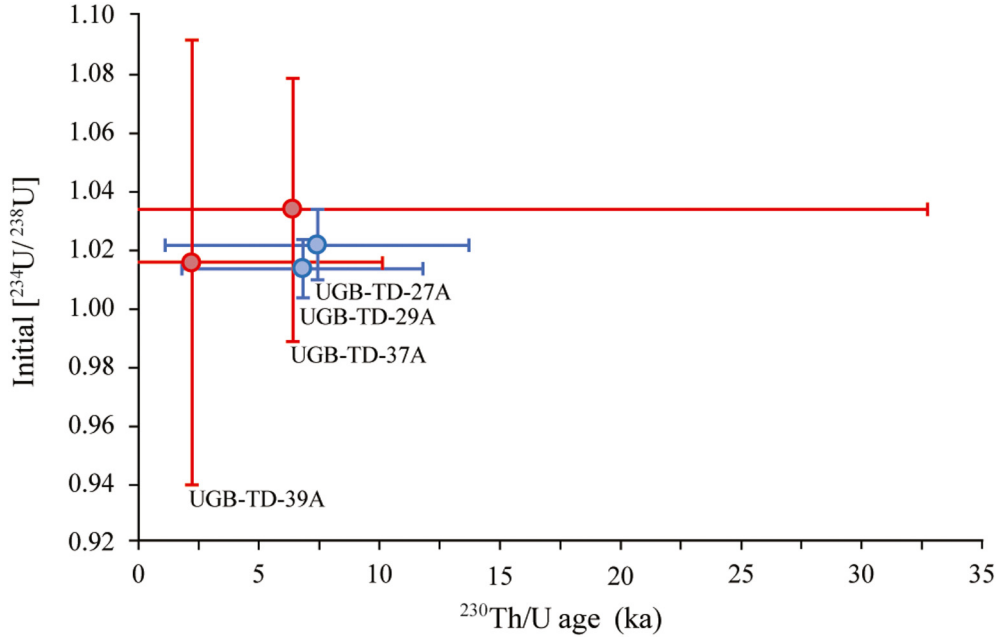

Fig. 6. ^{230}Th/U ages calculated from U-series isotope data plotted against initial [^{234}U/^{238}U] activity ratios. Blue symbols indicate samples from Giant Geyser and red symbols indicate samples from Castle Geyser. Error bars are shown at the 95% confidence level (±2σ). All data are compiled in a USGS data release (Churchill et al., 2020). (For interpretation of the references to colour in this figure legend, the reader is referred to the web version of this article.)

sample UGB-TD-31 a separated pine needle is older (3.3 cal ka BP) than the age for its bulk organic matter (1.9 cal ka BP) (Table 1).

3.2. Uranium-Thorium isotopes

The four samples of sinter from Giant and Castle Geysers have U concentrations ranging from 0.16 to 0.34 μg g^{-1} with similar Th concentrations (0.06 to 0.24 μg g^{-1}). Those concentrations are similar to median values in opal reported from a number of worldwide locations (0.44 μg g^{-1} for U and 0.20 μg g^{-1} for Th; $N = 57$; Gaillou et al., 2008) despite the very low dissolved U concentrations in Yellowstone thermal water samples (0.000001 to 0.000026 μg g^{-1} measured in 11 samples from geysers across the UGB; Paces et al., 2015). The similarity of U and Th concentrations in sinter samples resulted in elevated [^{232}Th/^{238}U]. Square brackets are used to denote activity ratios obtained by multiplying measured atomic ratios by the appropriate radioactive decay constants for ^{230}Th and ^{234}U (Cheng et al., 2013), and ^{232}Th and ^{238}U (Steiger and Jäger, 1977).

Measurable amounts of common thorium (^{232}Th) present in sinter samples imply that some ^{230}Th is not associated with the in-situ decay of parent isotope ^{234}U. Unlike hexavalent U, tetravalent Th is highly insoluble in aqueous solutions, thus any common ^{232}Th present in sinter samples is assumed to originate as detrital contaminant. To avoid calculating erroneously old ^{230}Th/U ages, any initial ^{230}Th incorporated along with detrital ^{232}Th at the time of sinter formation must be eliminated. This was done mathematically based on the measured [^{232}Th/^{238}U] and an assumption about the isotopic composition of the common thorium-bearing detrital component (Ludwig and Paces, 2002), which is assumed to be uniform and have an atomic Th/U of 4 with the following activity ratios and 2σ errors: [^{232}Th/^{238}U] = 1.276 ± 0.64; [^{234}U/^{238}U] = 1.0 ± 0.1; and [^{230}Th/^{238}U] = 1.0 ± 0.25. Corrected [^{230}Th/^{238}U] and [^{234}U/^{238}U] were used to calculate ^{230}Th/U ages, initial [^{234}U/^{238}U], and associated errors using conventional U-series age equations (Ludwig, 2012). Age uncertainties are propagated such that samples with little or no common Th (low [^{232}Th/^{238}U] values) will have small age errors essentially defined by analytical uncertainties, whereas samples with large [^{232}Th/^{238}U] values will require large corrections resulting in large age errors due to the substantial uncertainty (±50%) assigned to the "true" composition of the detrital component.

All 4 analyses of Yellowstone sinter yielded calculable, mid-Holocene ^{230}Th/U ages ranging from 2 to 7 ka, albeit with very large uncertainties (Fig. 6). Two samples from Giant Geyser (UGB-TD-27A and -29A) have statistically indistinguishable ^{230}Th/U ages of 7.4 ± 6.3 ka and 6.8 ± 5.0 ka that together yield a weighted average of 7.0 ± 3.8 ka. Age estimates for samples from Castle Geyser have substantially larger uncertainties due to their higher Th concentrations and [^{232}Th/^{238}U] values. Sample UGB-TD-37A requires the largest correction for initial ^{230}Th, but nevertheless yields a calculated ^{230}Th/U age similar to those for Giant Geyser (6.4 ± 26 ka), albeit with an age uncertainty far beyond being useful for defining reliable age relations. Data for Castle Geyser sample UGB-TD-39A implies a younger age of about 2.2 ± 7.9 ka, but again remains indistinguishable from other results given its large age uncertainty.

All samples yield analytically indistinguishable initial [^{234}U/^{238}U] values with a weighted mean value of 1.016 ± 0.007, defined largely by the more precisely determined results from the Giant Geyser samples. That value is close to being in radioactive secular equilibrium, which is expected under conditions involving aggressive water/rock interaction that result in bulk dissolution of U from host rock rather than preferential leaching of more soluble ^{234}U compared to ^{238}U. Existing [^{234}U/^{238}U] data for modern Yellowstone thermal water are scarce due in large part to the difficulty in accurate isotope measurements in water with very low U concentrations. Data reported elsewhere for Daisy and Oblong Geysers (Fig. 1b) suggests similarly low [^{234}U/^{238}U] values ranging from 0.86 to 1.24 with a mean value of 1.08 ± 0.24 (± 2 × standard deviation, $N = 7$; Paces et al., 2015).

3.3. Cosmogenic Beryllium-10

For the four samples collected for cosmogenic ^{10}Be exposure dating, repeated etchings of milled sinter in 2% HF and 1% HNO_3 were effective in progressively reducing major cation concentrations (Al, Ca, Na, Fe, Ti), thus indicating increased purification of opal (Churchill et al., 2020). Repeated etchings of the opal also reduced trace amounts of Be measurable via ICP-OES, which may reflect removal of meteoric ^{10}Be adhering

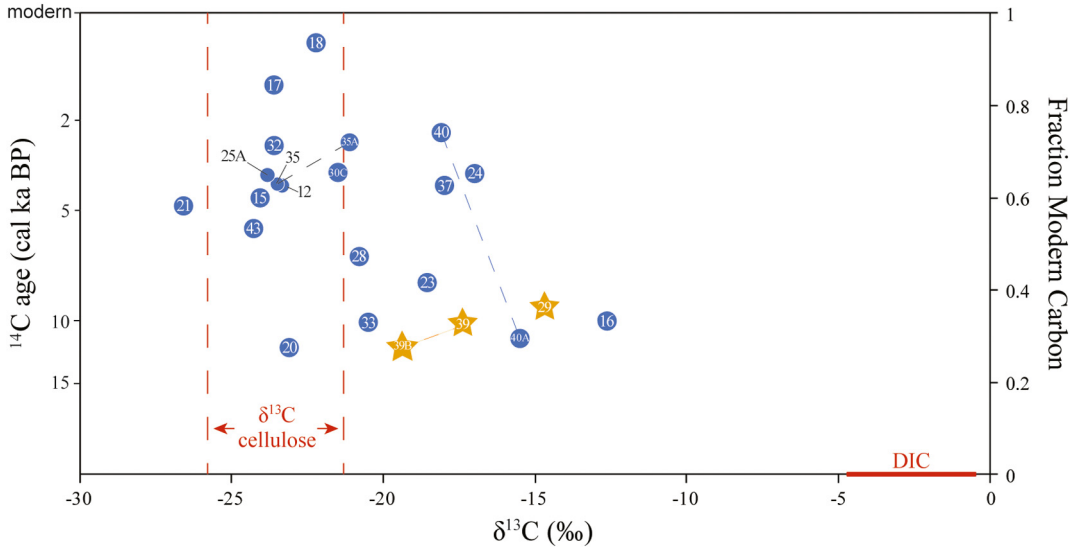

Fig. 7. $\delta^{13}C$ of organic material separated from the UGB sinter samples versus the fraction of modern carbon (right Y-axis) and implied ^{14}C age (left Y-axis). The $\delta^{13}C$ range for cellulose is from Loader et al. (2003) and the values for dissolved inorganic carbon (DIC) are from Bergfeld et al. (2019). Numbers inside each symbol are the respective sample IDs (Table 1). Dashed tie lines between symbols connect replicates. Orange stars indicate samples collected from the top of Giant Geyser (UGB-TD-29) and Castle Geyser (UGB-TD-39). All data are compiled in a USGS data release (Churchill et al., 2020).

to the opal grain surfaces. However, these etchings also considerably diminished the mass of the samples, and one sample (YGT18-30) completely dissolved after six etchings. Only one sample, YGT18-27 from the shield of Castle Geyser (Fig. 4b), yielded an opal fraction that was sufficiently large and pure enough to permit effective extraction of Be by ion-exchange methods. Sample YGT18-27 returned an apparent exposure age of 596 ± 18 ka (Table 1). The cosmogenic ^{10}Be exposure age for sample YGT18-27 was calculated using a calibration of regional in situ ^{10}Be production rates based on measurements at Promontory Point, Utah (Lifton et al., 2015). The nuclide- and time-

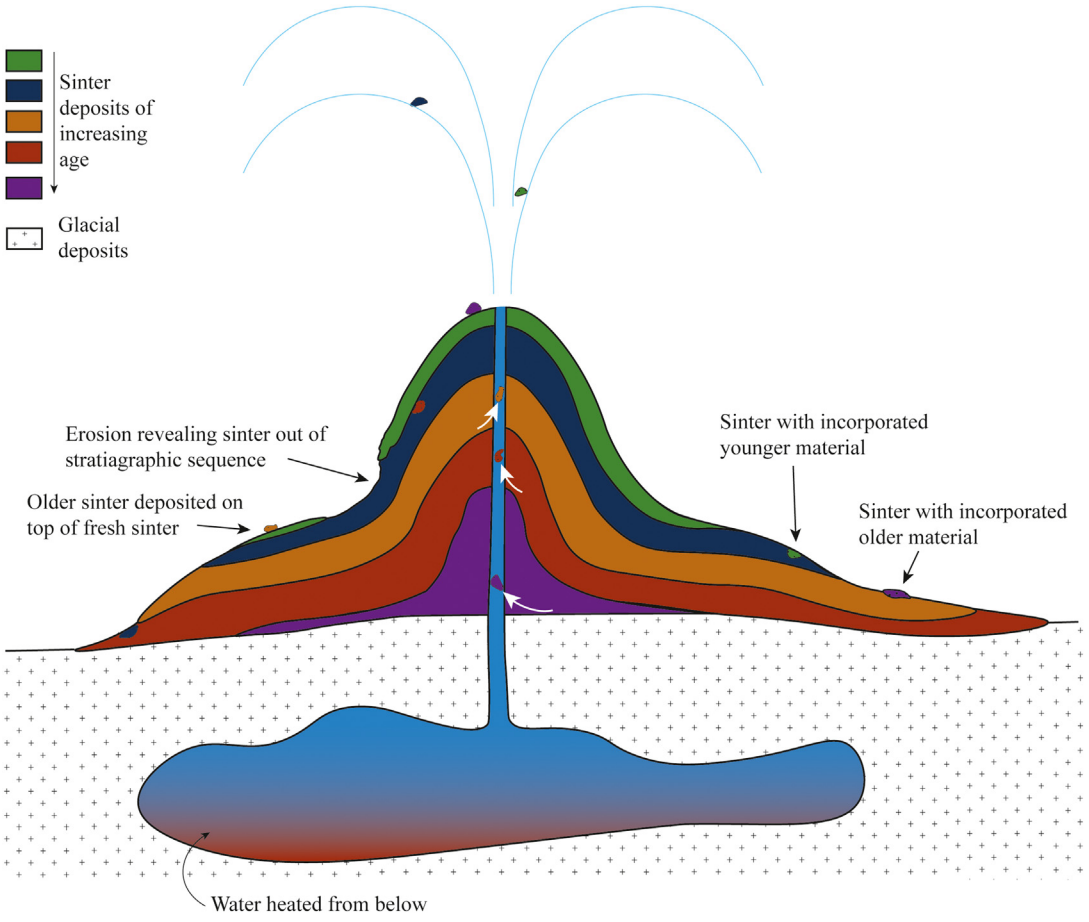

Fig. 8. A schematic illustration showing various ways in which sinter can be physically mixed, resulting in radiocarbon ages that do not correlate with original deposition age.

dependent 'LSDn' scaling model formulated by Lifton et al. (2014) is implemented in the age calculations. Exposure ages were derived from the CRONUS-Earth calculator version 3 (Balco et al., 2008). Snowpack data are not available for the Upper Geyser Basin and sinter surface erosion rates are also not known in the field area; hence the exposure ages were not corrected for snow shielding or erosion.

4. Discussion

Most previous studies using ^{14}C to date post-glacial sinter deposits either relied on a limited number of samples, were restricted by relatively small sample sizes which did not allow for $\delta^{13}C$ analysis of the organic material, or both (e.g., Lutz et al., 2002; Lynne et al., 2005; Foley, 2006; Lynne et al., 2008; Lowenstern et al., 2016). Furthermore, replicate ^{14}C analyses from individual specimens were not attempted and well-defined stratigraphic information allowing comparison of relative chronologies was mostly not included, although other authors have noted ^{14}C ages that did not correspond to stratigraphic position (Lynne et al., 2008). To avoid some of these shortcomings, we attempted to collect a large number of samples for ^{14}C analysis, mostly along well-defined stratigraphic sections. We also analyzed replicates from several samples, and when enough carbon was available, we analyzed for $\delta^{13}C$.

The large number of ^{14}C and $\delta^{13}C$ data that we present have some significant problems, highlighting that radiocarbon dating of sinter deposits is not as straightforward as previously assumed. Radiocarbon age estimates for samples from Riverside (Fig. 2), Giant (Fig. 3), and Castle (Fig. 4) Geysers are not consistent with their associated stratigraphic positions. For example, the ^{14}C ages obtained from samples collected at the top of Giant (UGB-TD-29; Fig. 3a) and Castle (UGB-TD-39; Fig. 4a) Geysers represent the most recently deposited material, yet they yield the oldest radiocarbon ages (9.4 and 12.1 cal ka BP, respectively; Table 1) at each geyser. Similarly, ^{14}C ages from the bottom of Giant (UGB-TD-24) and Castle (UGB-TD-31) Geysers, which should represent the oldest deposits, yield some of the youngest ages (3.8 and 1.5 cal ka BP, respectively). Additionally, multiple sub-sample replicates of organic material separated from several individual samples result in significantly different ages far beyond their reported analytical errors (Table 1, Fig. 5).

Organic material trapped in the sinter could originate externally, meaning outside of the deposit itself (e.g., pollen, needles, charcoal, leaves, etc.), or as in-situ microbial mats growing synchronously with sinter layers. Most sinter contains both forms of organic material, but in different proportions. In the few cases where we were able to separate charcoal from the bulk of the sample, there were significant differences between the ages of the charcoal and the corresponding bulk sample. Also, the age of the separated charcoal piece from sample UGB-TD-37 is older than the charcoal from sample UGB-TD-35 (Table 1), although it is from a stratigraphically higher position (Fig. 4a), and therefore should be younger.

As geysers erupt, silica is continuously deposited on top of the microbial mats, encasing and eventually silicifying the bacteria (e.g., Jones and Renaut, 2003; Campbell et al., 2015a). This process kills the bacteria, but it does not fully replace it, and so biologic signatures are left behind which can later be identified (Campbell et al., 2015b). For example, at Champagne Pool in New Zealand, bacterial and archaeal lipids were found preserved in silica sinter for at least 9000 years (Kaur et al., 2011). At the Krýsuvík hot spring in Iceland, approximately half the sinter thickness is attributed to silicified microorganisms that form alternating laminae of microbial layers and laminated silica layers devoid of microbes (Konhauser et al., 2001).

Whereas typical $\delta^{13}C$ values of cyanobacteria range from −20 to −25‰ (Sakata et al., 1997; Jahnke et al., 2004) and tree cellulose values range from −22 to −26‰ (Loader et al., 2003), microbial mats that grow in geothermal areas commonly have significantly heavier (less negative) $\delta^{13}C$ values, ranging up to −5‰ (Jennings et al., 2017). This is due to bacterial fixation of dissolved inorganic carbon (DIC) present in the thermal water that supplies the sinter deposits (Schidlowski, 2000; van der Meer et al., 2003; van Der Meer et al., 2007; Jennings et al., 2017). The DIC in thermal water has a geological origin and hence is devoid of ^{14}C. Consequently, older apparent ages can be obtained for samples containing this type of microbial organic material. The $\delta^{13}C$ values of many UGB sinter samples (12 out of 23, or 52%) have $\delta^{13}C$ values heavier than −22‰ (Table 1), suggesting that a significant portion of the dispersed (bulk) organic material consists of microbial mats that fixed DIC (Fig. 7). A study done in El Tatio, Chile similarly found organic material with heavy $\delta^{13}C$ values in sinter and excluded the contaminated samples from their radiocarbon age results (Muñoz-Saez et al., 2020).

The concentrations of dissolved CO_2 in UGB thermal waters are relatively low (<3.4 mmol/kg; Hurwitz et al., 2016), and the CO_2 is most likely sourced either from the underlying magma, or from the Paleozoic limestone that covered much of the region prior to Yellowstone volcanism (Christiansen, 2001). The ^{14}C concentration in either a magmatic or Paleozoic sedimentary source is essentially zero, and the $\delta^{13}C$ of the DIC measured in Yellowstone waters ranges between −4.7 to −0.7‰ (Bergfeld et al., 2019; Fig. 7). The $\delta^{13}C$ of travertine deposited from thermal water flowing through the Paleozoic limestone is even heavier, ranging from 2.7 to 5.2‰ (Fouke et al., 2000). Thus, carbon in UGB sinter samples is likely a mixture of modern carbon with light (more negative) $\delta^{13}C$ compositions and ancient, ^{14}C-depleted carbon with heavy $\delta^{13}C$ compositions depending on the proportions of carbon from external versus in-situ sources. The $\delta^{13}C$ and ^{14}C values are scattered (Fig. 7) because microbial DIC fractionation can yield a wide range of isotopic values (Jennings et al., 2017). Furthermore, physical mixing can change carbon isotope compositions. This can happen when old sinter pieces are reincorporated into new deposits (Lynne et al., 2008), or if sinter dissolution by meteoric water leads to the transport of the released carbon to a different stratigraphic position (Fig. 8). Because there are multiple carbon sources within a single sinter sample, all these factors can combine to result in unreliable radiocarbon ages.

The four sinter samples analyzed for U and Th isotopes are poor U-series dating candidates given their very low U concentrations and elevated amounts of common Th (^{232}Th). Low U concentrations in siliceous sinter are consistent with the very low concentrations of U present in UGB thermal water, which are presumed to be a consequence of reducing conditions in the hydrothermal reservoir. Those conditions favor tetravalent U species that are highly insoluble in aqueous solutions. Although all four samples yield ages consistent with post-glacial deposition (that is, ca. 15 ka; Licciardi and Pierce, 2018), their very large $^{230}Th/U$ age uncertainties, caused by substantial corrections for presence of initial ^{230}Th, preclude their use for paleoenvironmental or hydrothermal reconstruction. Nevertheless, the fact that all four analyses yielded concordant $^{230}Th/U$ ages that are consistent with the overall range of radiocarbon ages implies that post-depositional mobility of U may not be a major issue in these materials. Additional geochemical screening of sinter samples to determine those that might have U concentrations and U/Th values more amenable to U-series dating may allow increased precision in future studies. Application of this method may become more important as deposits reach or exceed the ~45 ka limit of the radiocarbon system.

In contrast to the post-glacial ages that were calculated using the ^{14}C and U-series data, the single sample dated using cosmogenic ^{10}Be data (YGT18-27) yields an exposure age of 596 ± 18 ka (Table 1). This age is older than the radiometric ages of all the underlying rhyolite flows in the UGB (Christiansen, 2001). The most common explanation for anomalously old cosmogenic nuclide exposure ages is inheritance of isotopes accumulated during prior exposure of surfaces (Gosse and Phillips, 2001). However, hundreds of thousands of years of prior exposure is not plausible for surface deposits in the UGB because older deposits are likely to have been removed by Pinedale-aged glacial erosion beneath the >1 km thick ice cap over the Yellowstone Plateau

(Pierce, 1979; Licciardi et al., 2001; Licciardi and Pierce, 2018). We therefore attribute the erroneously old exposure age to contamination by non-cosmogenic ^{10}Be. Based on well-established protocols for chemical preparation of purified crystalline quartz for cosmogenic ^{10}Be measurements (e.g., Kohl and Nishiizumi, 1992), we are confident that repeated etchings of the opal in 2% HF and 1% HNO_3 would have removed all meteoric ^{10}Be that may have resided on the surfaces of the unetched opal grains. Thus, we suspect the anomalously high concentration of ^{10}Be in the sample is most likely due to contamination by meteoric ^{10}Be trapped in the molecular water in the opal structure or in interstices in the sinter. Furthermore, because the concentration of molecular water in the opal decreases as sinter matures from opal-A to quartz (Herdianita et al., 2000), non-cosmogenic ^{10}Be concentrations would also vary accordingly. Although repeated etchings of the opal succeeded in reducing the concentration of major cations and trace amounts of Be measurable via ICP-OES, not all of the meteoric ^{10}Be could be eliminated with rigorous etching because the entire sample would dissolve. This meteoric-sourced ^{10}Be can overprint the very small amount of cosmogenic ^{10}Be in late Pleistocene to Holocene-age surfaces, thereby making it impossible to obtain a reliable exposure age.

Cosmogenic ^{10}Be measurements are most commonly made in crystalline quartz, which can be effectively isolated and purified from rocks using well-established methods. We therefore suggest that future attempts to date siliceous sinter using cosmogenic ^{10}Be will depend on the presence of quartz grains, and thus should focus on older sinter deposits which are more likely to have quartz (Lynne et al., 2007). By the time sinter has diagenetically transformed from opal-A to quartz, it has expelled nearly all the water from its structure (Herdianita et al., 2000), thus any ^{10}Be found in the quartz should be almost entirely cosmogenic in origin. It should therefore be possible to separate quartz of diagenetic origin from the sinter and successfully purify it to isolate the cosmogenic ^{10}Be for measurement. However, because the transition to quartz takes tens of thousands of years (Herdianita et al., 2000), ^{10}Be exposure dating of quartz-bearing sinter is likely not applicable to late Pleistocene and Holocene deposits such as those in the UGB. Future studies will be required to test the potential of ^{10}Be exposure dating of older sinter in other settings.

The results presented here suggest that great care must be used when interpreting ages of post-glacial sinter deposits in active hydrothermal areas because of their significant implications. Hydrothermal explosions are among the most common geologic hazards at YNP, but despite their significance, dating post-glacial hydrothermal explosions has been extremely difficult (Morgan et al., 2009), often because age estimates rely on very limited numbers of samples containing extremely small charcoal fragments. Hence reliable dating of sinter in hydrothermal explosion deposits is critical for assessing their hazard (Christiansen et al., 2007). Similarly, there is a debate regarding the interpretation of ^{14}C ages associated with a large volcanic eruption in the Taupo Volcanic Zone in New Zealand. Holdaway et al. (2018) propose that the Taupo eruption age of 232 $\pm$ 10 CE derived from a tree killed by the erupted ignimbrite was affected by ^{14}C-depleted (magmatic) CO_2, whereas Hogg et al. (2019) suggest that the "*claim that the Pureora and other near-source dates are anomalously old is flawed*". Although the eruptive event in question does not involve hydrothermal deposits, these ambiguities highlight the uncertainties associated with radiocarbon-dating young (post-glacial) events in active magmatic and hydrothermal environments where contamination with ^{14}C-depleted components is possible.

5. Conclusions

Based on the analysis of many silica sinter samples using ^{14}C, along with complementary U-series and cosmogenic ^{10}Be dating methods, we demonstrate that there are significant challenges to determining the timing of major post-glacial geologic events using these hydrothermal deposits. Each of the methods we applied was hampered by a different cause. In the case of ^{14}C, we propose that the most significant problem is incorporation of microbial mats that metabolize old carbon present in thermal groundwater. With the application of U-series, we conclude that very low uranium concentrations and U/Th values in sinter samples cause significant problems for obtaining precise dating results. For cosmogenic ^{10}Be exposure, the anomalously old age most likely results from contamination by meteoric ^{10}Be trapped in the sinter. This meteoric source can overprint the very small amount of cosmogenic ^{10}Be, thereby making it impossible to obtain a reliable exposure age. By considering the limitations of the different methods applied and presented in this study, we hope that this cautionary tale will lead to a more systematic approach which could improve the ability to date hydrothermal silica deposits associated with geyser activity.

CRediT authorship contribution statement

Dakota M. Churchill: Investigation, Writing - original draft, Data curation, Visualization. **Michael Manga:**Conceptualization, Investigation, Validation, Resources, Writing - original draft, Supervision, Funding acquisition. **Shaul Hurwitz:**Conceptualization, Validation, Investigation, Resources, Writing - original draft, Supervision, Funding acquisition, Project administration. **Sara Peek:**Investigation, Validation, Data curation, Writing - review & editing. **Joseph M. Licciardi:**Investigation, Resources, Validation, Funding acquisition, Writing - original draft. **James B. Paces:**Investigation, Resources, Validation, Writing - original draft.

Acknowledgements

This study was conducted under Research Permits YELL-2018-SCI-8030 and YELL-2018-SCI-5910. We thank Annie Carlson, Jeff Hungerford, Erin White, Behnaz Hosseini and Bill Keller from the Yellowstone Center for Resources for help in the field and with logistics. We thank Alan Hidy at LLNL-CAMS, Avriel Schweinsberg at the University at Buffalo, and Debra Driscoll at SUNY College of Environmental Science and Forestry for help with data acquisition and interpretation. We thank the KCCAMS staff for use of their radiocarbon dating facilities. Chris Schiller and Cathy Whitlock at Montana State University are thanked for separating charcoal and a needle from the samples, and Sam Segal at the University of New Hampshire is thanked for help with ^{10}Be sample processing. We thank Bill Evans and two anonymous reviewers for constructive comments. S. Hurwitz, S. Peek and J.B. Paces were funded by the USGS Volcano Hazards Program. M. Manga and D.M. Churchill were funded by NSF 1724986 and the Esper Larsen fund. Any use of trade, firm, or product names is for descriptive purposes only and does not imply endorsement by the U.S. Government.

Declaration of competing interest

The authors declare that they have no known competing financial interests or personal relationships that could have appeared to influence the work reported in this paper.

References

Abedini, A.A., Robinson, J.E., Muffler, L.J., White, D.E., Beeson, M.H., Truesdell, A.H., 2015. Database for the geologic map of Upper Geyser Basin, Yellowstone National Park, Wyoming. U.S. Geological Survey Data Series 911, scale 1:4,800, doi:https://doi.org/10.3133/ds911.

Amelin, Y., Back, M., 2006. Opal as a U–Pb geochronometer: search for a standard. Chem. Geol. 232, 67–86. https://doi.org/10.1016/j.chemgeo.2006.02.018.

Balco, G., Stone, J.O., Lifton, N.A., Dunai, T.J., 2008. A complete and easily accessible means of calculating surface exposure ages or erosion rates from ^{10}Be and ^{26}Al measurements. Quat. Geochronol. 3, 174–195. https://doi.org/10.1016/j.quageo.2007.12.001.

Bergfeld, D., Lowenstern, J.B., Hunt, A.G., Hurwitz, S., McCleskey, B.R., Peek, S.E., 2019. Chemical and isotopic data on gases and waters for thermal and non-thermal features across Yellowstone National Park (ver. 2.0, March 2019). U.S. Geol. Survey Data Release https://doi.org/10.5066/F7H13105.

Campbell, K.A., Lynne, B.Y., 2006. Diagenesis and dissolution at Sinter Island (456 years BP), Taupo volcanic zone: silica stars and the "birth" of quartz. Proceedings 28th New Zealand Geothermal Workshop, p. 7.

Campbell, K.A., Buddle, T.F., Browne, R.L., 2004. Late Pleistocene silica sinter associated with fluvial, lacustrine, volcaniclastic and landslide deposits at Tahunaatara, Taupo Volcanic Zone, New Zealand. Earth Environ. Sci. Trans. R. Soc. Edinburgh 94, 485–501. https://doi.org/10.1017/S0263593300000833.

Campbell, K.A., Guido, D.M., Gautret, P., Foucher, F., Ramboz, C., Westall, F., 2015a. Geyserite in hot-spring siliceous sinter: Window on Earth's hottest terrestrial (paleo) environment and its extreme life. Earth Sci. Rev. 148, 44–64. https://doi.org/10.1016/j.earscirev.2015.05.009.

Campbell, K.A., Lynne, B.Y., Handley, K.M., Jordan, S., Farmer, J.D., Guido, D.M., Foucher, F., Turner, S., Perry, R.S., 2015b. Tracing biosignature preservation of geothermally silicified microbial textures into the geological record. Astrobiology 15, 858–882. https://doi.org/10.1089/ast.2015.1307.

Chen, Y., Gao, J., Feng, J., 1993. ESR dating of geyserites from intermittent geyser sites on the Tibetan plateau. Appl. Radiat. Isot. 44, 207–213. https://doi.org/10.1016/0969-8043(93)90221-U.

Cheng, H., Edwards, R.L., Shen, C-C, Polyak, J., Asmerom, Y., Woodhead, J., Hellstrom, J., Wang, Y., Kong, X., Spötl, C., Wang, X., and Alexander Jr., E.C., 2013. Improvements in ^{230}Th dating, ^{230}Th and ^{234}U half-life values, and U–Th isotopic measurements by multi-collector inductively coupled plasma mass spectrometry. Earth Planet. Sci. Lett., 371–372, 82–91, doi:https://doi.org/10.1016/j.epsl.2013.04.006.

Christiansen, R.L., 2001. The Quaternary and Pliocene Yellowstone Plateau volcanic field of Wyoming, Idaho, and Montana. U.S. Geol. Surv. Prof. Pap. 729-G, 146. https://doi.org/10.3133/pp729G.

Christiansen, R.L., Lowenstern, J.B., Smith, R.B., Heasler, H., Morgan, L.A., Nathenson, M., Mastin, L.G., Muffler, L., Robinson, J.E., 2007. Preliminary assessment of volcanic and hydrothermal hazards in Yellowstone National Park and vicinity. U.S. Geol. Survey Open-File Rep. 2007–1071, 94. https://pubs.usgs.gov/of/2007/1071/.

Churchill, D.M., Peek, S., Hurwitz, S., Manga, M., Damby, D.E., Conrey, R., Paces, J.B., Licciardi, J.M., 2020. Mineralogy, chemistry and isotope composition of silica sinter deposits from the Upper Geyser Basin, Yellowstone National Park. U.S. Geol. Survey Data Release https://doi.org/10.5066/P90SU3TV.

Corbett, L.B., Bierman, R., Rood, D.H., 2016. An approach for optimizing in situ cosmogenic ^{10}Be sample preparation. Quat. Geochronol. 33, 24–34. https://doi.org/10.1016/j.quageo.2016.02.001.

Foley, D., 2006. Dating Castle Geyser: preliminary results and broad speculations on the geologic development of geysers and hydrothermal systems in Yellowstone National Park, Wyoming, USA. Trans. — Geotherm. Res. Council 30, 413–417.

Fouke, B.W., Farmer, J.D., Des Marais, D.J., Pratt, L., Sturchio, N.C., Burns, C., Discipulo, M.K., 2000. Depositional facies and aqueous-solid geochemistry of travertine-depositing hot springs (Angel Terrace, Mammoth Hot Springs, Yellowstone National Park, USA). J. Sediment. Res. 70, 565–585. https://doi.org/10.1306/2dc40929-0e47-11d7-8643000102c1865d.

Fournier, R.O., 1985. The behavior of silica in hydrothermal solutions. Rev. Econ. Geol. 2, 45–61.

Gaillou, E., Delaunay, A., Rondeau, B., Bouhnik-le-Coz, M., Fritsch, E., Cornen, G., Monnier, C., 2008. The geochemistry of gem opals as evidence of their origin. Ore Geol. Rev. 34, 113–126. https://doi.org/10.1016/j.oregeore2007.07.004.

Gosse, J.C., Phillips, F.M., 2001. Terrestrial in situ cosmogenic nuclides: theory and application. Quat. Sci. Rev. 20, 1475–1560. https://doi.org/10.1016/S0277-3791(00)00171-2.

Guidry, S.A., Chafetz, H.S., 2003. Depositional facies and diagenetic alteration in a relict siliceous hot-spring accumulation: examples from Yellowstone National Park, USA. J. Sediment. Res. 73, 806–823. https://doi.org/10.1306/022803730806.

Herdianita, N.R., Browne, P.R.L., Rodgers, K.A., Campbell, K.A., 2000. Mineralogical and textural changes accompanying ageing of silica sinter. Mineral. Deposita 35, 48–62. https://doi.org/10.1007/s001260050005.

Hogg, A., Wilson, C.J., Lowe, D.J., Turney, C., White, P., Lorrey, A.M., Manning, S.W., Palmer, J.G., Bury, S., Brown, J., Southon, J., Petchey, F., 2019. Correspondence: the Taupo eruption occurred in 232±10 CE, and not later. Nat. Commun. https://doi.org/10.31223/osf.io/7r5jp.

Holdaway, R.N., Duffy, B., Kennedy, B., 2018. Evidence for magmatic carbon bias in ^{14}C dating of the Taupo and other major eruptions. Nat. Commun. 9, 4110. https://doi.org/10.1038/s41467-018-06357-0.

Howald, T., Person, M., Campbell, A., Lueth, V., Hofstra, A., Sweetkind, D., Gable, C.W., Banerjee, A., Luijendijk, E., Crossey, L., Karlstrom, K., 2014. Evidence for long timescale (>103 years) changes in hydrothermal activity induced by seismic events. Geofluids 15, 252–268. https://doi.org/10.1111/gfl.12113.

Hurwitz, S., Lowenstern, J.B., 2014. Dynamics of the Yellowstone hydrothermal system. Rev. Geophys. 51, 375–411. https://doi.org/10.1002/2014RG000452.

Hurwitz, S., Manga, M., 2017. The fascinating and complex dynamics of geyser eruptions. Annu. Rev. Earth Planet. Sci. 45, 31–59. https://doi.org/10.1146/annurev-earth-063016-015605.

Hurwitz, S., Hunt, A.G., Evans, W.C., 2012. Temporal variations of geyser water chemistry in the Upper Geyser Basin, Yellowstone National Park, USA. Geochem. Geophys. Geosyst. 13 (12), Q12005. https://doi.org/10.1029/2012GC004388.

Hurwitz, S., Clor, L.E., McCleskey, R.B., Nordstrom, D.K., Hunt, A.G., Evans, W.C., 2016. Dissolved gases in hydrothermal (phreatic) and geyser eruptions at Yellowstone National Park. USA. Geology 44, 235–238. https://doi.org/10.1130/G37478.1.

Jahnke, L.L., Embaye, T., Hope, J., Turk, K.A., Van Zuilen, M., Des Marais, D.J., Farmer, J.D., Summons, R.E., 2004. Lipid biomarker and carbon isotopic signatures for stromatolite-forming, microbial mat communities and Phormidium cultures from Yellowstone National Park. Geobiology 2, 31–47. https://doi.org/10.1111/j.1472-4677.2004.00021.x.

Jennings, R.D.M., Moran, J.J., Jay, Z.J., Beam, J., Whitmore, L.M., Kozubal, M.A., Kreuzer, H.W., Inskeep, W., 2017. Integration of metagenomic and stable carbon isotope evidence reveals the extent and mechanisms of carbon dioxide fixation in high-temperature microbial communities. Front. Microbiol. 8, 88. https://doi.org/10.3389/fmicb.2017.00088.

Jones, B., Renaut, R.W., 2003. Hot spring and geyser sinters: the integrated product of precipitation, replacement, and deposition. Can. J. Earth Sci. 40, 1549–1569. https://doi.org/10.1139/e03-078.

Kaur, G., Mountain, B.W., Hopmans, E.C., Pancost, R.D., 2011. Preservation of microbial lipids in geothermal sinters. Astrobiology 11, 259–274. https://doi.org/10.1089/ast.2010.0540.

Kohl, C., Nishiizumi, K., 1992. Chemical isolation of quartz for measurement of in-situ-produced cosmogenic nuclides. Geochim. Cosmochim. Acta 56, 3583–3587. https://doi.org/10.1016/0016-7037(92)90401-4.

Konhauser, K.O., Phoenix, R., Bottrell, S.H., Adams, D.G., Head, I.M., 2001. Microbial-silica interactions in Icelandic hot spring sinter: possible analogues for some Precambrian siliceous stromatolites. Sedimentology 48, 415–433. https://doi.org/10.1046/j.1365-3091.2001.00372.x.

Licciardi, J.M., 2000. Alpine Glacier and Pluvial Lake Records of Late Pleistocene Climate Variability in the Western United States. [Ph.D. dissertation]. Oregon State University, Corvallis, p. 155.

Licciardi, J.M., Pierce, K.L., 2018. History and dynamics of the Greater Yellowstone Glacial System during the last two glaciations. Quat. Sci. Rev. 200, 1–33. https://doi.org/10.1016/j.quascire2018.08.027.

Licciardi, J.M., Clark, U., Brook, E.J., Pierce, K.L., Kurz, M.D., Elmore, D., Sharma, P., 2001. Cosmogenic ^{3}He and ^{10}Be chronologies of the late Pinedale northern Yellowstone ice cap, Montana, USA. Geology 29, 1095–1098. https://doi.org/10.1130/0091-7613(2001)029<1095:CHABCO>2.0.CO;2.

Lifton, N., Sato, T., Dunai, T.J., 2014. Scaling in situ cosmogenic nuclide production rates using analytical approximations to atmospheric cosmic-ray fluxes. Earth Planet. Sci. Lett. 386, 149–160. https://doi.org/10.1016/j.epsl.2013.10.052.

Lifton, N., Caffee, M., Finkel, R., Marrero, S., Nishiizumi, K., Phillips, F.M., Goehring, B., Gosse, J., Stone, J., Schaefer, J., Theriault, B., 2015. In situ cosmogenic nuclide production rate calibration for the CRONUS-Earth project from Lake Bonneville, Utah, shoreline features. Quat. Geochronol. 26, 56–69. https://doi.org/10.1016/j.quageo.2014.11.002.

Loader, N.J., Robertson, I., McCarroll, D., 2003. Comparison of stable carbon isotope ratios in the whole wood, cellulose and lignin of oak tree-rings. Palaeogeogr. Palaeoclimatol. Palaeoecol. 196, 395–407. https://doi.org/10.1016/S0031-0182(03)00466-8.

Lowe, D.R., Braunstein, D., 2003. Microstructure of high-temperature (> 73 °C) siliceous sinter deposited around hot springs and geysers, Yellowstone National Park: the role of biological and abiological processes in sedimentation. Can. J. Earth Sci. 40, 1611–1642. https://doi.org/10.1139/e03-066.

Lowenstern, J.B., Hurwitz, S., McGeehin, J., 2016. Radiocarbon dating of silica sinter deposits in shallow drill cores from the Upper Geyser Basin, Yellowstone National Park. J. Volcanol. Geotherm. Res. 310, 132–136. https://doi.org/10.1016/j.jvolgeores.2015.12.005.

Ludwig, K.R., 2012. User's Manual for Isoplot 3.75, A Geochronological Toolkit for Microsoft Excel. vol. 5. Berkeley Geochronological Center Special Publication, p. 75.

Ludwig, K.R., Paces, J.B., 2002. Uranium-series dating of pedogenic silica and carbonate, Crater Flat, Nevada. Geochim. Cosmochim. Acta 66, 487–506. https://doi.org/10.1016/S0016-7037(01)00786-4.

Lutz, S.J., Caskey, S.J., Mildenhall, D.D., Browne, R.L., Johnson, S.D., 2002, January. Dating sinter deposits in northern Dixie Valley, Nevada—the paleoseismic record and implications for the Dixie Valley geothermal system. Proceedings 27th Workshop on Geothermal Reservoir Engineering, pp. 284–290.

Lynne, B.Y., 2012. Mapping vent to distal-apron hot spring paleo-flow pathways using siliceous sinter architecture. Geothermics 43, 3–24. https://doi.org/10.1016/j.geothermics.2012.01.004.

Lynne, B.Y., Campbell, K.A., Moore, J., Browne, R.L., 2005. Diagenesis of 1900-year-old siliceous sinter (opal-A to quartz) at Opal Mound, Roosevelt Hot Springs, Utah, U.S.A. Sediment. Geol. 119, 249–278. https://doi.org/10.1016/j.sedgeo.2005.05.012.

Lynne, B.Y., Campbell, K.A., James, B.J., Browne, P.R., Moore, J., 2007. Tracking crystallinity in siliceous hot-spring deposits. Am. J. Sci. 307, 612–641. https://doi.org/10.2475/03.2007.03.

Lynne, B.Y., Campbell, K.A., Moore, J., Browne, R.L., 2008. Origin and evolution of the Steamboat Springs siliceous sinter deposit, Nevada, U.S.A. Sediment. Geol. 210, 111–131. https://doi.org/10.1016/j.sedgeo.2008.07.006.

Lynne, B.Y., Heasler, H., Jaworowski, C., Foley, D., Smith, I.J., Smith, G.J., Sahdarani, D., 2017. Using ground penetrating radar, scanning electron microscopy and thermal infrared imagery to document near-surface hydrological changes in the Old Faithful Geyser area, Yellowstone National Park, U.S.A. Geothermics 68, 33–53. https://doi.org/10.1016/j.geothermics.2017.02.007.

Maher, K., Wooden, J.L., Paces, J.B., Miller, D.M., 2007. ^{230}Th–U dating of surficial deposits using the ion microprobe (SHRIMP-RG): a microstratigraphic perspective. Quat. Int. 166, 15–28. https://doi.org/10.1016/j.quaint.2007.01.003.

Morgan, L.A., Shanks, W.C., Pierce, K.L., 2009. Hydrothermal processes above the Yellowstone magma chamber: large hydrothermal systems and large hydrothermal explosions. Geol. Soc. Am. Spec. Pap. 459. https://doi.org/10.1130/SPE459.

Muffler L.J., White, D.E., Beeson, M.H., and Truesdall, A.H., 1982. Geologic map of Upper Geyser Basin, Yellowstone National Park, Wyoming. U.S. Geological Survey Miscellaneous Geologic Investigations Map, I-1371, scale 1:4,800.

Muñoz-Saez, C., Manga, M., Hurwitz, S., Slagter, S., Churchill, D.M., Reich, M., Damby, D., Morata, D., 2020. Radiocarbon dating of silica sinter and postglacial hydrothermal activity in the El Tatio geyser field. Geophys. Res. Lett. https://doi.org/10.1029/2020GL087908.

Nemchin, A.A., Neymark, L.A., Simons, S.L., 2006. U-Pb SHRIMP dating of uraniferous opals. Chem. Geol. 227, 113–132. https://doi.org/10.1016/j.chemgeo.2005.09.005.

Neymark, L.A., Paces, J.B., 2013. Ion-probe U–Pb dating of authigenic and detrital opal from Neogene-Quaternary alluvium. Earth Planet. Sci. Lett. 361, 98–109. https://doi.org/10.1016/j.epsl.2012.11.037.

Neymark, L.A., Amelin, Y., Paces, J.B., Peterman, Z.E., 2002. U-Pb ages of secondary silica at Yucca Mountain, Nevada: implications for the paleohydrology of the unsaturated zone. Appl. Geochem. 17, 709–734. https://doi.org/10.1016/S0883-2927(02)00032-X.

Paces, J.B., Neymark, L.A., Wooden, J.L., Persing, H.M., 2004. Improved spatial resolution for U-series dating of opal at Yucca Mountain, Nevada, USA, using ion-microprobe and microdigestion methods. Geochim. Cosmochim. Acta 68, 1591–1606. https://doi.org/10.1016/j.gca.2003.08.022.

Paces, J.B., Neymark, L.A., Whelan, J.F., Wooden, J.L., Lund, S., Marshall, B.D., 2010. Limited hydrologic response to Pleistocene climate change in deep vadose zones — Yucca Mountain, Nevada. Earth Planet. Sci. Lett. 300, 287–298. https://doi.org/10.1016/j.epsl.2010.10.006.

Paces, J.B., Long, A.J., Koth, K., 2015. Potential Application of Radiogenic Isotopes and Geophysical Methods to Understand the Hydrothermal System of the Upper Geyser Basin, Yellowstone National Park. vol. 1077. National Park Service, Natural Resource Report NPS/YELL/NRR, p. 57. https://doi.org/10.13140/RG.2.1.2049.9922.

Paces, J.B., Palmer, M.V., Palmer, A.N., Long, A.J., Emmons, M.P., 2020. 300,000 yr. history of water-table fluctuations at Wind Cave, South Dakota, USA—Scale, timing, and groundwater mixing in the Madison Aquifer. Geol. Soc. Am. Bull. 132, 1447–1468. https://doi.org/10.1130/B35312.1.

Pierce, K.L., 1979. History and dynamics of glaciation in the northern Yellowstone National Park area. U.S. Geol. Surv. Prof. Pap. 729-F, 91. https://doi.org/10.3133/pp729F.

Reimer, J., Bard, E., Bayliss, A., Beck, J.W., Blackwell, G., Bronk Ramsey, C., Buck, C.E., Cheng, H., Edwards, R.L., Friedrich, M., Grootes, M., Guilderson, T., Haflidason, H., Hajdas, I., Hatté, C., Heaton, T.J., Hoffmann, D.L., Hogg, A.G., Hughen, K.A., Kaiser, K.F., Kromer, B., Manning, S.W., Niu, M., Reimer, R.W., Richards, D.A., Scott, E.M., Southon, J.R., Staff, R.A., Turney, C.S.M., van der Plicht, J., 2013. IntCal13 and Marine13 radiocarbon age calibration curves 0–50,000 years cal BP. Radiocarbon 55, 1869–1887. https://doi.org/10.2458/azu_js_rc.55.16947.

Sakata, S., Hayes, J.M., McTaggart, A.R., Evans, R.A., Leckrone, K.J., Togasaki, R.K., 1997. Carbon isotopic fractionation associated with lipid biosynthesis by a cyanobacterium: relevance for interpretation of biomarker records. Geochim. Cosmochim. Acta 61, 5379–5389. https://doi.org/10.1016/S0016-7037(97)00314-1.

Schidlowski, M., 2000. Carbon isotopes and microbial sediments. Microbial Sediments. Springer, Berlin, Heidelberg, pp. 84–95 https://doi.org/10.1007/978-3-662-04036-2_11.

Sharp, W.D., Ludwig, K.R., Chadwick, O.A., Amundson, R., Glaser, L.L., 2003. Dating fluvial terraces by ^{230}Th/U on pedogenic carbonate, Wind River Basin, Wyoming. Quat. Res. 59, 139–150. https://doi.org/10.1016/S0033-5894(03)00003-6.

Slagter, S., Reich, M., Munoz-Saez, C., Southon, J., Morata, D., Barra, F., Gong, J., Skok, J.R., 2019. Environmental controls on silica sinter formation revealed by radiocarbon dating. Geology 47, 330–334. https://doi.org/10.1130/G45859.1.

Steiger, R.H., Jäger, E., 1977. Subcommission on geochronology: convention on the use of decay constants in geo-and cosmochronology. Earth Planet. Sci. Lett. 36, 359–362. https://doi.org/10.1016/0012-821X(77)90060-7.

Stuiver, M., Reimer, J., 1993. Extended ^{14}C database and revised CALIB radiocarbon calibration program. Radiocarbon 35, 215–230.

van der Meer, M.T., Schouten, S., Damsté, J.S.S., de Leeuw, J.W., Ward, D.M., 2003. Compound-specific isotopic fractionation patterns suggest different carbon metabolisms among Chloroflexus-like bacteria in hot-spring microbial mats. Appl. Environ. Microbiol. 69, 6000–6006. https://doi.org/10.1128/AEM.69.10.6000-6006.

van Der Meer, M.T., Schouten, S., Damsté, J.S.S., Ward, D.M., 2007. Impact of carbon metabolism on ^{13}C signatures of cyanobacteria and green non-sulfur-like bacteria inhabiting a microbial mat from an alkaline siliceous hot spring in Yellowstone National Park (USA). Environ. Microbiol. 9, 482–491. https://doi.org/10.1111/j.1462-2920.2006.01165.x.